HHS Public Access

Author manuscript

Cell. Author manuscript; available in PMC 2019 January 11.

Published in final edited form as:

Cell. 2018 January 11; 172(1-2): 68–80.e12. doi:10.1016/j.cell.2017.12.004.

Allosteric Coupling of Drug Binding and Intracellular Signaling in the A_{2A} Adenosine Receptor

Matthew T. Eddy[1,2], **Ming-Yue Lee**[2], **Zhan-Guo Gao**[3], **Kate L. White**[2], **Tatiana Didenko**[1], **Reto Horst**[1,4], **Martin Audet**[2], **Pawel Stanczak**[1], **Kyle M. McClary**[2], **Gye Won Han**[2], **Kenneth A. Jacobson**[3], **Raymond C. Stevens**[2], and **Kurt Wüthrich**[1,5,‡,*]

[1]Department of Integrative Structural and Computational Biology, The Scripps Research Institute, 10550 North Torrey Pines Road, La Jolla, CA 92037, USA

[2]Departments of Biological Sciences and Chemistry, Bridge Institute, University of Southern California, Los Angeles, CA 90089, USA

[3]Laboratory of Bioorganic Chemistry, NIDDK, National Institutes of Health, Bethesda, Maryland 20892, USA

[4]Pfizer Worldwide Research and Development, Eastern Point Road, Groton, CT, USA

[5]Skaggs Institute of Chemical Biology, The Scripps Research Institute, 10550 North Torrey Pines Road, La Jolla, CA 92037, USA

Abstract

Signaling across cellular membranes, the 826 human G protein-coupled receptors (GPCR) govern a wide range of vital physiological processes, making GPCRs prominent drug targets. X-ray crystallography provided GPCR molecular architectures, which also revealed the need for additional structural dynamics data to support drug development. Here, NMR with the wild type-like A_{2A} receptor (A_{2A}AR) in solution provides a comprehensive characterization of signaling-related structural dynamics. All six tryptophan indole and eight glycine backbone ^{15}N–^{1}H NMR signals in A_{2A}AR were individually assigned. These NMR probes provided insight into the role of $Asp52^{2.50}$ as an allosteric link between the orthosteric drug binding site and the intracellular signaling surface, revealing strong interactions with the toggle switch $Trp\ 246^{6.48}$, and delineated the structural response to variable efficacy of bound drugs across A_{2A}AR. The present data

‡Corresponding author: wuthrich@scripps.edu.
*Lead Contact

Author Contributions

M.T.E. carried out protein production and sample purification and recorded the NMR spectra; M.T.E. and K.W. analyzed the NMR data with input from T.D., P.S. and R.H.; Z.G., K.A.J., and K.L.W. performed the radioligand binding assays; M.T.E. and K.M.M. produced A_{2A}AR-BRIL for crystal structure determination; M.T.E., M-Y.L., and M.A. crystallized A_{2A}AR-BRIL; G.W.H. and M-Y.L. solved the A_{2A}AR-BRIL crystal structure; M.T.E., R.C.S and K.W. designed the project; M.T.E. and K.W. prepared the manuscript with input from all the authors.

Supplemental Information

Supplemental Information includes STAR methods, seven figures, and three tables.

support GPCR signaling based on dynamic interactions between two semi-independent subdomains connected by an allosteric switch at Asp52$^{2.50}$.

Graphical Abstract

Monitoring dynamics of GPCR signaling using stable isotope NMR reveals the path of communication enabling an allosteric response to ligand binding.

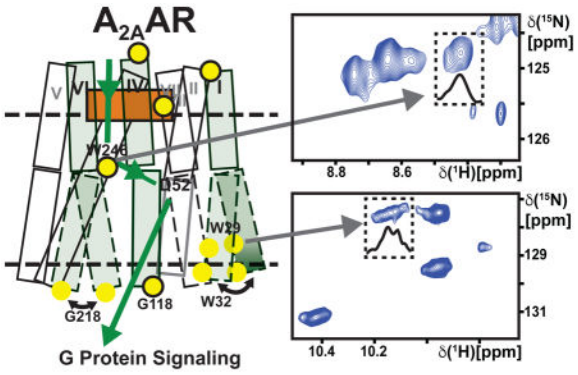

Introduction

Drug binding in G protein-coupled receptors (GPCRs) initiates signaling across cell membranes over a distance of about 30 Ångstroms (Audet and Bouvier, 2012; Rosenbaum et al., 2009). From the molecular architecture of GPCRs, as determined by X-ray crystallography, it is clear that this signal transfer must be supported by dynamic plasticity of the receptors, which needs to be investigated by other methods. NMR spectroscopy in solution complements GPCR crystal structure determination by its unique ability of detecting multiple, simultaneously populated conformational states, as has been reported, for example, in studies of the β_2–adrenergic receptor (β_2AR) (Bokoch et al., 2010; Eddy et al., 2016; Horst et al., 2013; Kim et al., 2013; Kofuku et al., 2012; Kofuku et al., 2014; Liu et al., 2012a; Manglik et al., 2015; Nygaard et al., 2013), the μ-opioid receptor (MOR) (Okude et al., 2015; Sounier et al., 2015), the β_1–adrenergic receptor (Isogai et al., 2016), and the human A_{2A} adenosine receptor (A_{2A}AR) (Ye et al., 2016). Thereby, drugs bound in the orthosteric pocket can alter the relative populations of two or multiple locally different conformational states on the intracellular surface, which signal to partner proteins (Didenko et al., 2013; Manglik and Kobilka, 2014). Here, these potentialities of NMR in solution were used to investigate the structural basis of the functional role of Asp52$^{2.50}$ (superscripts indicate the Ballesteros-Weinstein nomenclature; (Ballesteros and Weinstein, 1995), which has been reported to be a key residue in an allosteric switch along the 30-Ångstrom signaling pathway from the drug binding pocket of A_{2A}AR to its intracellular surface (Figure 1A).

The key role of Asp52$^{2.50}$ in regulating signaling to intracellular partner proteins has been experimentally documented for over 30 different class A GPCRs (Katritch et al., 2014). Asp52$^{2.50}$ is also one of the most highly conserved residues, with aspartic acid at this position in about 85% of the approximately 700 class A GPCRs in the human proteome

(Figure 1B) (Katritch et al., 2014). For some GPCRs, replacement of Asp52$^{2.50}$ with an uncharged amino acid resulted in marked decrease of G protein signaling; examples include the cannabinoid receptors CB1 and CB2 (Tao and Abood, 1998) and the type 1 neurotensin receptor (NTSR1) (Martin et al., 1999). For other receptors, including the angiotensin II receptor (Bihoreau et al., 1993), MOR (Xu et al., 1999) and A_{2A}AR (Massink et al., 2014), replacement of Asp52$^{2.50}$ has been reported to completely abolish G protein signaling. In addition to its role in regulating G protein signaling, Asp52$^{2.50}$ was seen in high-resolution crystal structures of A_{2A}AR and DOR to form coordinative bonds with a sodium ion (Liu et al., 2012b), which provided an initial rationale for independently observed physiological effects of sodium ions on opiate ligand binding and receptor signaling (Cooper et al., 1982; Pert et al., 2009).

A_{2A}AR belongs to the purinergic receptor family that binds endogenous adenosine and regulates vasodilation and inflammation (Ohta and Sitkovsky, 2001), and affects the central nervous system (Dunwiddie and Masino, 2001). A_{2A}AR is a validated target for the treatment of Parkinson's disease (Bara-Jimenez et al., 2003), and more recently it has been identified as a potential therapeutic target for cancer immunotherapies (Young et al., 2016). Relating to this biomedical interest, A_{2A}AR has been subject to intense studies, including crystal structure determinations of complexes with antagonists (Doré et al., 2011; Jaakola et al., 2008) and agonists (Lebon et al., 2011; Xu et al., 2011), and for a ternary complex of A_{2A}AR with an agonist and a "mini-G_S" G protein mimetic (Carpenter et al., 2016).

A recent crystal structure determination of the variant receptor A_{2A}AR[D52N] in complex with the full agonist UK432097 (PDB 5W5F) showed that this structure is nearly identical to that of the A_{2A}AR complex with the same agonist (PDB 3QAK) (Xu et al., 2011), including nearly identical conformations of the intracellular signaling surfaces. In this paper we further explore the structural basis of the Asp52$^{2.50}$-related allosteric effects on the receptor function, showing that NMR in solution can provide novel insights. Based on sequence-specific assignment of numerous amino acid residues distributed throughout the receptor (Figures 1C and S1), we report observations of a strong interplay between Asp52$^{2.50}$ and the "toggle switch" tryptophan at position 246$^{6.48}$ (Rosenbaum et al., 2009; Schwartz et al., 2006; Shi et al., 2002), and of local structural polymorphisms on the A_{2A}AR intracellular surface which can be directly related to the functionality of the Asp52$^{2.50}$ allosteric switch.

Results

We obtained sequence-specific resonance assignments for well-resolved resonances in the NMR spectra of A_{2A}AR (Figure 1D), including the indole ^{15}N–^{1}H-signals of all six tryptophans (Figure 1E) and the backbone ^{15}N–^{1}H signals of eight glycines (Figure 1F). The assigned signals provided NMR probes of conformation in the hydrophobic core, at the extracellular surface with the entry to the orthosteric ligand binding cavity, and at the intracellular surface (Figure 1C). The labeling also included helix VI, which has been observed in crystal structures to undergo a large structural rearrangement, relative to an antagonist complex, upon formation of a complex with an agonist (Xu et al., 2011) and in a ternary complex with an agonist and a G protein or G protein mimetic (Carpenter et al., 2016). We then investigated the response of the assigned NMR signals to variable efficacy of

bound drugs. To obtain information on the allosteric switch at Asp52$^{2.50}$, we compared corresponding NMR data of A_{2A}AR and A_{2A}AR[D52N], where the allosteric center is known to be inactive (Massink et al., 2014). This experimental approach was based on the use of a novel expression system for GPCRs, which allowed us to obtain sequence-specific NMR assignments by single-residue amino acid replacements.

Expression of Stable-Isotope-Labeled A_{2A}AR in *Pichia pastoris*

A_{2A}AR was expressed in *Pichia pastoris,* which enabled uniform labeling with the stable isotopes ^{2}H,^{13}C and ^{15}N. The use of extensive deuteration provided the expected improvement of the A_{2A}AR NMR spectra (Figure S2), which made the present project feasible. Optimization of each step of the expression and purification process resulted in the capability to routinely produce milligram-per-liter quantities of homogeneous isotope-labeled A_{2A}AR (see STAR Methods). A_{2A}AR reconstituted into LMNG/CHS mixed micelles for NMR studies was highly homogeneous, as observed by analytical SEC, which showed that samples were monodisperse and did not contain detectable amounts of aggregated protein (Figure S3B).

To ensure that the present solution NMR studies were performed with A_{2A}AR that was pharmacologically and structurally identical to A_{2A}AR produced in the widely used *Sf9* cells (Carpenter et al., 2016; Jaakola et al., 2008; Xu et al., 2011), we performed extensive characterization of A_{2A}AR produced from *Pichia*. Ligand binding experiments performed with A_{2A}AR which was either embedded in membranes isolated from *Pichia* preparations (Figure S3, C and D) or reconstituted in LMNG/CHS micelles (Figure S3A) showed nearly identical activity to A_{2A}AR produced in *Sf9* cells. A crystal structure of *Pichia*-produced A_{2A}AR in complex with the antagonist ZM241385 was found to be identical to an earlier corresponding structure of A_{2A}AR produced in *Sf9* (Figure S3, E and F).

Sequence-Specific Resonance Assignments in A_{2A}AR

Uniform stable-isotope labeling with ^{15}N and ^{2}H enabled the recording of A_{2A}AR NMR spectra where all tryptophan indole ^{15}N–^{1}H and most glycine backbone ^{15}N–^{1}H NMR signals were well separated from the other signals (Figures 1, E and F). In addition, the signals numbered 1 to 30 in the 2D [^{15}N,^{1}H]-TROSY correlation spectrum (Figure 1D) were also well separated, so that chemical shift changes or variations of the line shapes could readily be detected. Primary assignments were obtained for the A_{2A}AR complex with the antagonist ZM2411385, based on comparisons of the spectra of A_{2A}AR and A_{2A}AR variants containing single-residue amino acid replacements. Throughout, we checked that the native globular fold was preserved in the variant proteins, by monitoring the chemical shifts of the signals 1 to 30 (Figure 1D) as illustrated for the tryptophan assignments with the Figures S4 to S6 and Table S2.

The Trp indole ^{15}N–^{1}H signals were assigned from the missing peak for the variant A_{2A}AR in which the corresponding tryptophan was replaced (Figure 2, A and B). The signal for Trp129$^{4.50}$ was weaker than the other signals, but was reproducibly observed in multiple sample preparations and was present in the spectra of all variants with a different tryptophan replacement. Replacement of Trp246$^{6.48}$ with Phe resulted in a missing signal outside of the

tryptophan indole ^{15}N–^{1}H spectral region (Figures 1E and 2B); this outlying chemical shift is due to large ring current fields in the chemical environment of Trp246$^{6.48}$, as confirmed by ring current calculations based on corresponding A_{2A}AR crystal structures (Table S1) (Johnson Jr and Bovey, 1958; Koradi et al., 1996; Liu and Wüthrich, 2016; MacDonald and Phillips, 1967; Perkins and Wüthrich, 1979; Wüthrich, 1969; Wüthrich, 1986).

Backbone ^{15}N–^{1}H signals of eight glycines were assigned by single-residue replacements of Gly with Ala (Figure 2, C–I). Overall, assignment of the Gly signals was straightforward, since, with the sole exception of Gly 5$^{1.31}$, they were strong and well resolved.

Extensive deuteration has first been achieved with soluble proteins in the late 1960s (Markley et al., 1968), and it became mandatory with the introduction of transverse relaxation-optimized spectroscopy (TROSY) for studies of large structures (Pervushin et al., 1997). A limitation arising from the use of $^{2}H_2O$ as the solvent during protein expression is that back-protonation of the amide groups may be incomplete. While all six Trp indole ^{15}N–^{1}H signals expected in A_{2A}AR were observed, *albeit* with low intensity for Trp129 (Figures 1 and 2), we could therefore not so far establish whether or not the TROSY spectrum of Figure 1D includes signals from all residues in the polypeptide chain. In this situation, we selected 30 well-resolved polypeptide backbone signals, which all represent large conformation-dependent ^{1}H chemical shifts and are therefore sensitive probes of conformational rearrangements (Wüthrich, 1986), to monitor the preservation of the overall three-dimensional fold in the variant A_{2A}ARs used for the NMR assignments (Figures S4–S6; Table S2).

Interplay of the “Toggle Switch” Tryptophan 246$^{6.48}$ with the Allosteric Center at Asp52$^{2.50}$

Tryptophan 246$^{6.48}$ is referred to in the GPCR literature as the “toggle switch” or “rotamer toggle switch”, since early studies predicted large changes in the rotamer state of Trp246$^{6.48}$ between GPCR complexes with agonists and antagonists (Nygaard et al., 2013; Shi et al., 2002). Trp246$^{6.48}$ is located in helix VI at the bottom of the ligand-binding cavity (Figure 1). Variations in the conformation of Trp$^{6.48}$ between antagonist and agonist complexes have been widely observed in crystal structures of class A human GPCRs (Rosenbaum et al., 2009), including A_{2A}AR (Jaakola et al., 2008; Xu et al., 2011) and very recently the human CB1 receptor (Hua et al., 2017).

As was done for the other tryptophan indole ^{15}N–^{1}H signals, a sequence-specific assignment for Trp246$^{6.48}$ was obtained for the A_{2A}AR complex with the antagonist ZM241385 (Figures 2B and 3A). This ring current-shifted signal outside of the characteristic Trp indole ^{15}N–^{1}H spectral region can be expected to be highly sensitive to local conformational rearrangements, since these may cause large chemical shift changes (Johnson Jr and Bovey, 1958; MacDonald and Phillips, 1967; Wüthrich, 1969; Wüthrich, 1986). The NMR signal of Trp246$^{6.48}$ in A_{2A}AR complexes with agonists was therefore *de novo* identified by amino acid replacement (Figure 3B), revealing a large chemical shift change relative to complexes with antagonists (Figure 3A). Table S1 shows that the observed chemical shift change is in good qualitative agreement with the difference between the ring current shifts calculated from the crystal structures. Within the expected accuracy of ring current shift analyses (Perkins and Wüthrich, 1979; Wüthrich, 1986), this observation established direct

correlations for conformational changes near Trp246$^{6.48}$ between inactive and active-like states of A_{2A}AR seen in solution and in crystal structures (Figure 4A).

In view of the high sensitivity of the indole ^{15}N–^{1}H chemical shift of Trp246$^{6.48}$ to local conformational rearrangements, we established *de novo* resonance assignments also for the variant protein A_{2A}AR[D52N]. Two-residue variants were thus prepared, where in addition to Asp52$^{2.50}$, Trp246$^{6.48}$ was replaced by phenylalanine. This showed that there are large chemical shifts between complexes of the two proteins with antagonists (Figure 3, A and C) and agonists (Figure 3, B and D). Furthermore, there are large chemical shift differences of the Trp246$^{6.48}$ NMR signal between the complexes with agonists and antagonists for A_{2A}AR (Figure 3, A and B), and A_{2A}AR[D52N] (Figure 3, C and D). Response to variable efficacy of bound drugs is thus preserved in A_{2A}AR[D52N], where the allosteric switch is known to be inactivated (Massink et al., 2014).

Considering the close proximity of Asp52$^{2.50}$ to the orthosteric ligand binding site (Figure 1C), we further checked the response to bound drugs with similar efficacy but different chemical structures (Figure 3E). Closely similar chemical shift differences were observed between complexes with different combinations of agonists and antagonists (Figure S7), indicating that the observed NMR spectral changes were indeed a response to different drug efficacies, rather than being due to direct contacts with the different ligand chemical structures (Figure 3E).

Overall, the data in Figure 3 reveal a tight interplay between the toggle switch Trp246$^{6.48}$ and the allosteric center at Asp52$^{2.50}$, as manifested by the large chemical shift differences between the spectra of A_{2A}AR and A_{2A}AR[D52N] with corresponding ligands (Figure 3). We further see that inactivation of the allosteric center does not abolish the response of the toggle switch Trip246$^{6.48}$ indole ^{15}N–^{1}H signal to variable efficacy of drugs bound to the orthosteric site.

Assigned NMR Signals Manifest Specific Response on the Intracellular A_{2A}AR Surface to Variable Efficacy of Bound Drugs

In contrast to the large ring current shifts for the Trp246$^{6.48}$ indole ^{15}N–^{1}H signal, ring current shifts calculated for the remaining Trp ^{15}N–^{1}H indole groups were much smaller for all complexes studied (Table S1), and the ring current shift calculations predicted measureable chemical shift changes between antagonist and agonist complexes only for Trp29$^{1.55}$ (Table S1). For glycine residues in A_{2A}AR, at most very small ring current shifts of the backbone ^{15}N–^{1}H signals were calculated. The results shown in Figures 4, E–G, and 5 thus appear to be in line with recent observations on ^{19}F-NMR probes in GPCRs, which indicated that large chemical shift changes between different functional states of GPCRs can be expected only in locations where the observed NMR signals originate from atom groups experiencing sizeable ring current fields (Liu and Wüthrich, 2016).

To investigate the response to variable efficacy of bound drugs, we recorded 2D [^{15}N,^{1}H]-TROSY correlation spectra of [u-^{15}N,~70% ^{2}H]-A_{2A}AR complexes with six ligands of different pharmacological efficacies (Figure 3E) for which crystal structures are available (Carpenter et al., 2016; Doré et al., 2011; Jaakola et al., 2008; Lebon et al., 2011; Xu et al.,

2011). Figure 4D affords a survey of the response to drugs of different efficacies seen at the assigned tryptophan indole ^{15}N–^{1}H and glycine backbone ^{15}N–^{1}H signals. Between agonist and antagonist complexes, significant changes were observed for 11 of the 14 assigned residues, i.e., either ^{1}H or ^{15}N chemical shift differences greater than 0.05 ppm and 0.20 ppm, respectively, or changes in signal fine structure.

Details of the response to variable drug efficacy indicated in Figure 4D are shown in Figure 4, E–K, for Trp indole ^{15}N–^{1}H resonances and in Figure 5 for Gly backbone ^{15}N–^{1}H resonances. For Trp29$^{1.55}$ we observe multiple components in the NMR signal for complexes with antagonists, and a single component for the agonist complex. There are small chemical shift changes which result in partial overlap of the signals for Trp29$^{1.55}$ and Trp143 in the agonist spectra, whereas two clearly separated signals are seen in the spectra of antagonist complexes. Trp268$^{7.33}$ shows a single resonance component throughout. Its chemical shift is invariant among the three antagonist complexes, and we observe very small ^{1}H chemical shift variations among the three agonist complexes. For Trp129$^{4.50}$ the data of Figure 2A shows that the resonance is very weak in the complex with the antagonist ZM241385. We conclude that this is due to incomplete back-protonation of the indole ^{15}N-^{1}H group, since there is no evidence of excessive line broadening. In the other complexes, the Trp129$^{4.50}$ NMR line was not detected, indicating that the back exchange was less efficient than in the complex with ZM241385.

Gly118$^{4.39}$ shows a relatively large response to ligand efficacy, with an approximately 1 ppm shift in the ^{15}N dimension between complexes with agonists and antagonists that indicates a change in local backbone conformation at the intracellular end of helix IV. Gly114 in ICL2 presents small chemical shift changes in the ^{15}N and ^{1}H dimensions between complexes with ligands of different efficacies. Gly142$^{4.63}$ also shows a clear response to ligand efficacy, with chemical shift changes in both the ^{15}N and ^{1}H dimensions between complexes with different ligands. For Gly218 we observe two components of unequal intensities only in spectra of complexes with antagonists. In addition, there is a chemical shift change for Gly218 in the ^{15}N and ^{1}H dimensions between complexes with antagonists and agonists.

Inactivation of the Allosteric Center at Asp52$^{2.50}$ Modulates the Response to Variable Drug Efficacy at the A_{2A}AR Intracellular Surface

To investigate effects from inactivation of the allosteric center at Asp52$^{2.50}$ by replacement with Asn52$^{2.50}$, we recorded 2D [^{15}N,^{1}H]-TROSY correlation spectra of [u-^{15}N,~70% ^{2}H]-A_{2A}AR[D52N] complexes with the antagonist ZM241385 and the agonist NECA, and compared these data to spectra of the corresponding complexes with A_{2A}AR. A survey of the effects from this single-amino acid replacement observed by this comparison in Figure 6A shows that only the regions of the three-dimensional structure of A_{2A}AR from the toggle switch Trp246$^{6.48}$ to the intracellular surface are affected, whereas there is no response on the extracellular surface and at the orthosteric drug binding site.

Most signals located on the intracellular surface showed either differences in chemical shifts, NMR signal intensities, or fine structures between A_{2A}AR and A_{2A}AR[D52N]. For Gly218 we observed two resonance components in NMR spectra of A_{2A}AR-antagonist complexes, whereas in the A_{2A}AR[D52N]-antagonist complex only a single resonance component is

seen. The chemical shift of this single resonance is closely similar to the chemical shift of the upfield component in $A_{2A}AR$, and the resonance of Gly218 also shows an approximately 5-fold increase in intensity (Figure 6B). In the $A_{2A}AR$[D52N]-agonist complex, G218 also showed increased NMR signal intensity compared to the same $A_{2A}AR$ complex (Figure 6C). $Trp29^{1.55}$ showed a broad, relatively weak signal in $A_{2A}AR$ complexes with antagonists and agonists, and in spectra of $A_{2A}AR$-antagonist complexes two components are observed (Figures 4, H and I; 6D). In contrast, $Trp29^{1.55}$ in $A_{2A}AR$[D52N] shows only a single component in spectra of both the antagonist and agonist complexes (Figure 6, D and I). Also, the intensity of the $Trp29^{1.55}$ signal is about 5-fold more intense in $A_{2A}AR$[D52N]. For $Trp32^{1.58}$ in $A_{2A}AR$, we observed two resonance components in the agonist complexes (Figure 4, J and K), whereas for $A_{2A}AR$[D52N] only a single component was observed in the agonist complex (Figure 6E). As an illustration of the inert behavior of residues near the extracellular surface (Figure 6A), Figure 6, D and E, shows that Trp143 has the same chemical shift and signal intensity in spectra of $A_{2A}AR$ and $A_{2A}AR$[D52N] for both agonist and antagonist complexes.

Discussion

The result visualized in Figure 6A is highly intriguing in the context of literature data on allosteric coupling from G protein binding toward the drug binding sites in human GPCRs. Thus, studies of β_2AR led to the conclusion that complex formation with an intracellular partner protein allosterically modulated the conformation of the orthosteric drug binding cavity at the extracellular receptor surface (DeVree et al., 2016; Staus et al., 2016). Analogous observations were based on NMR spectroscopic studies of the β_1-adrenergic receptor (β_1AR) (Isogai et al., 2016). In the present study, inactivation of the allosteric center changes the conformational dynamics on the intracellular surface and does not affect the conformation or dynamics of the extracellular receptor surface (Figures 6). This suggests that the view of GPCRs consisting of two semi-independent subdomains, an orthosteric domain that reacts to varied molecular “triggers” and an intracellular domain where signaling pathways converge (Katritch et al., 2012; Venkatakrishnan et al., 2016), may also apply to $A_{2A}AR$, where the allosteric center links together the two regions through residue $Asp^{2.50}$.

In $A_{2A}AR$, as previously observed for other GPCRs (Eddy et al., 2016; Horst et al., 2013; Kim et al., 2013; Kofuku et al., 2014; Liu et al., 2012a; Manglik et al., 2015; Nygaard et al., 2013; Okude et al., 2015; Sounier et al., 2015), observations of local conformational polymorphisms by NMR spectroscopy in solution complement the available $A_{2A}AR$ crystal structures (Carpenter et al., 2016; Cheng et al., 2017; Doré et al., 2011; Jaakola et al., 2008; Lebon et al., 2011; Segala et al., 2016; Sun et al., 2017; Xu et al., 2011) with key insights into dynamic signaling-related processes. Comparison of agonist-bound crystal structures of $A_{2A}AR$ (PDB 3QAK) and $A_{2A}AR$[D52N] (PDB 5W5F) bound to the same agonist showed no structural differences at the intracellular surface, even though the two proteins demonstrated striking differences in G protein signaling. Thus, the presently discovered relations between the presence of local polymorphisms at the intracellular tips of helices I and VI and signaling at the intracellular surface (Figure 7) would have gone unnoticed without the use of solution NMR techniques.

A mechanism of how inactivation of the allosteric center could result in a loss of signaling may involve an interplay between Asp52$^{2.50}$ and Trp246$^{6.48}$, as the loss of signaling-related dynamics at the A_{2A}AR[D52N] intracellular surface (Figure 7) is correlated with changes in the local environment of Trp246$^{6.48}$ in A_{2A}AR[D52N] (Figure 3). The chemical shift of Trp246$^{6.48}$ is highly sensitive to the proximity and relative orientation of the nearby ring of Phe242$^{6.44}$ (Table S1); thus differences in the chemical shift of Trp246$^{6.48}$ between A_{2A}AR and A_{2A}AR[D52N] reflect changes in the relative orientation of these two residues between the native and variant proteins. Comparisons of inactive and active-like GPCRs have documented coupling of structural reorientation of Phe242$^{6.44}$ to structural rearrangements of helices associated with receptor activation (Elling et al., 2006; Rasmussen et al., 2011; Schwartz et al., 2006; Wacker et al., 2013). Thus, the present experimental evidence for reorientation of Phe242$^{6.44}$ in A_{2A}AR[D52N] may partly explain differences in signaling between A_{2A}AR and A_{2A}AR[D52N].

NMR studies of rhodopsin also provided support for an involvement of Trp$^{6.48}$ reorientation in driving changes at the intracellular surface. Specifically, studies of rhodopsin in the solid state revealed a reorientation of Trp$^{6.48}$ relative to the covalently bound retinal upon activation with light (Crocker et al., 2006), which is coupled with an outward reorientation of the intracellular end of helix VI as part of a proposed two-step activation mechanism (Kimata et al., 2016). Trp$^{6.48}$ has also been implicated in studies of so called “efficacy switches” whereby a single point mutation can modulate the efficacy of a bound ligand. In the chemokine receptor CCR5, the amino acid replacement G286F$^{7.42}$ converted some antagonists into full agonists (Steen et al., 2013). Based on molecular modeling, a proposed mechanism for this effect involved reorientation of Trp$^{6.48}$ (Steen et al., 2013). In the δ–opioid receptor (DOR), an efficacy switch was observed for the variant D$^{2.50}$N, which converted some antagonists into biased agonists (Fenalti et al., 2014). Based on the present results that Trp246$^{6.48}$ and Phe242$^{6.48}$ are reoriented in the D52$^{2.50}$N variant (Figure 3), we hypothesize that the efficacy switch in the DOR D$^{2.50}$N variant may involve a similar reorientation of Trp$^{6.48}$. As Trp$^{6.48}$ is thus clearly important for receptor activation, and because of the high sequence conservation of both Trp246$^{6.48}$ and Phe242$^{6.44}$ among class A GPCRs (Katritch et al., 2012), the indole ^{15}N-^{1}H resonance of Trp246$^{6.48}$ provides a highly sensitive probe for future NMR studies of class A GPCR activation mechanisms.

The current study provides a means for assessing the extent to which concepts of GPCR “microswitches” and “microdomains”, first described in early literature of rhodopsin photoactivation, can be extended to other class A receptors. GPCR microswitches are local clusters of highly conserved amino acids proximately located in the receptor, which undergo coordinated structural changes between inactive and active states. The concept of microswitches or “functional microdomains” emerged from earlier studies that applied optical spectroscopy and site-directed mutagensis to delineate contributions of specific amino acids to rhodopsin photoactivation (Fahmy et al., 1995; Franke et al., 1990; Lin and Sakmar, 1996; Sakmar and Fahmy, 1995). Of particular relevance to the current study is literature data that reported changes in UV-absorbance of tryptophan residues upon rhodopsin photoactivation (Lin and Sakmar, 1996). Trp126$^{3.41}$ and Trp265$^{6.48}$ in rhodopsin were observed to transition from more hydrophobic to more hydrophilic environments upon activation; in particular, Trp265$^{6.48}$ experienced the largest change in local environment

among all the rhodopsin tryptophans (Lin and Sakmar, 1996). Additional literature data correlated changes in interactions among rhodopsin transmembrane residues with varied functional responses (Beck et al., 1998; Han et al., 1998; Shieh et al., 1997), giving rise to the idea of "functional microdomains" (Lin et al., 2000). The present study corroborates the main ideas of functional microswitches and microdomains in the adenosine A_{2A} receptor and provides a more solid structural foundation with tools that were not available at the time of these earlier rhodopsin studies.

The observations presented in this study were made possible by a multi-parameter NMR characterization of the conformation and dynamics of a human GPCR in solution. Most earlier NMR studies of human GPCRs have utilized a smaller number of reporter groups introduced by chemical conjugation after protein production, including ^{19}F-NMR probes introduced by labeling of surface-exposed cysteine residues (Chung et al., 2012; Horst et al., 2013; Kim et al., 2013; Klein-Seetharaman et al., 1999; Liu et al., 2012a; Manglik et al., 2015), and $^{13}CH_3$-probes introduced by reductive methylation of lysine residues (Bokoch et al., 2010; Kofuku et al., 2012; Kofuku et al., 2014; Nygaard et al., 2013; Okude et al., 2015; Sounier et al., 2015). While these have been highly successful in providing information at targeted locations, the stable-isotope-labeling strategy used here provides a more comprehensive view of GPCR activation. For future studies, this approach provides an avenue for obtaining ever denser networks of assigned NMR signals for monitoring function-related conformational rearrangements in GPCRs at ever higher resolution.

With regard to the physiological relevance, it is of key importance that the present study used a construct of the human A_{2A}AR that was closely similar to the native receptor, i.e., it did not contain either thermostabilizing point mutations or fusion proteins inserted into receptor loops, as is extensively used to make GPCRs amenable for crystallographic studies and also applied to other experimental techniques. Eliminating thermostabilizing modifications enables one to obtain information of the global dynamics and plasticity of GPCRs. Thus, the present study provides a framework whereby dynamic processes at the intracellular surface can be observed in parallel to monitoring structural changes in other regions of the receptor.

STAR METHODS

CONTACT FOR REAGENT AND RESOURCE SHARING

Please direct any requests for further information or reagents to the Lead Contact Kurt Wüthrich (wuthrich@scripps.edu).

EXPERIMENTAL MODEL AND SUBJECT DETAILS

Microbes—*E. coli* cells were cultured in LB medium. *P. pastoris* cells were cultured in BMGY and BMMY media (see Protein Expression below).

METHODS DETAILS

Mutagenesis—PCR-based site-directed mutagenesis (QuickChange II, Strategene, CA), was used to generate variant A_{2A}ARs with single amino acid replacements. Primers for mutagenesis are listed in the Table S4.

Protein Expression—For production of A_{2A}AR for NMR studies, the gene encoding human A_{2A}AR(1–316) containing a point mutation to remove the only glycosylation site (N154Q), an N-terminal FLAG tag, and a 10 X C-terminal His tag was cloned into a pPIC9K vector (Invitrogen) at the BamHI and NotI restriction sites. The pharmacological response of this construct to binding of orthosteric ligands has been demonstrated to be unchanged from the WT sequence (Palmer and Stiles, 1997). We expressed all A_{2A}AR NMR samples in *Pichia pastoris* and demonstrated that the protein was functionally and structurally identical to A_{2A}AR expressed in insect cells by validating the pharmacological response of A_{2A}AR to orthosteric ligands and by crystal structure comparison of the antagonist ZM241385 complexes of A_{2A}AR expressed, respectively, in Sf9 (PDB 4EIY) and in *P. pastoris* (PDB 6QAF), both with the protein BRIL fused into ICL3 (Figure S3). The construct was introduced by electroporation into the BG12 strain of *Pichia pastoris* (Biogrammatics, Carlsbad, CA).

For production of A_{2A}AR for crystal structure determination, the employed construct was nearly identical to a previously published construct (Chun et al., 2012; Liu et al., 2012b) which contained a fusion with residues 1 to 106 of apo-cytochrome $b_{562,}$ in the place of the residues 209 to 218 in the ICL3, and was thermostabilized by the amino acid replacements M7W, H102I and K106L. The only differences to this earlier construct were the removal of an N-terminal HA leader sequence and the amino acid exchange N154Q.

Expression was screened by small-scale protein production and Western Blots, i.e. about fifteen clones per construct were grown in 4 mL cultures and protein production was assessed by anti-FLAG Western Blots. From these clones, the highest expressing clone was selected for future experiments. Glycerol stocks of the high expressing clone were used to inoculate a 5 mL starter culture in buffered minimal glycerol (BMGY) media, which was grown at 30 °C to an O.D. of 7–10 in a 15 mL culture tube. Cells were collected by centrifugation at 3000 × g for 10 minutes and used to inoculate 50 mL BMGY medium in a 250 mL baffled flask, which was grown at 30 °C to an O.D. of 15–20. This entire culture was then used to inoculate 500 mL BMGY media and allowed to grow at 30 °C to reach an O.D. of 15–20. Cells were collected by centrifugation at 3000 × g for 15 minutes and resuspended in buffered minimal methanol (BMMY) medium without methanol and the temperature was lowered to 27 °C. The cultures were allowed to shake for 3–4 hours to ensure complete metabolisation of glycerol before methanol was added to a final concentration of 0.5% w/v to induce protein expression. Two additional 0.5% w/v aliquots of methanol were added 12 and 24 hours after induction. Expression proceeded for a total of 36 hours until cells were harvested by centrifugation at 3500 × g for 15 minutes. The isolated cell pellets were frozen in liquid nitrogen and stored at −80 °C for future processing.

To generate deuterated, ^{15}N isotopically labeled A_{2A}AR samples, cells were adapted to increasing amounts of deuterium oxide in BMGY media at 30 °C over a period of about 9

days. Adapted cells were grown in BMGY media containing 99.8% D_2O and ^{15}N ammonium sulfate and protein expression was induced in BMMY media containing 99.8% D_2O and ^{15}N ammonium sulfate.

NMR Sample Preparation—$A_{2A}AR$-containing cell pellets were resuspended in lysis buffer (50 mM sodium phosphate pH 7.0, 100 mM NaCl, 5% glycerol (w/v), and protease inhibitor cocktail solution prepared in-house) and broken by two passes through a cell disruptor (Constant Systems) operating at 40,000 PSI. Membranes were isolated by ultracentrifugation at 200,000 × g.

Isolated membranes were resuspended in buffer (10 mM HEPES pH 7.0, 10 mM KCl, 20 mM $MgCl_2$, 1M NaCl) and treated with 1 mM theophylline, protease inhibitor cocktail solution (prepared in-house), and 2 mg/mL iodoacetamide 1 hour prior to solubilization. Protein was extracted from the membrane in buffer containing 0.5% (w/v) 2,2-didecylpropane-1,3-bis-β-*D*-maltopyranoside (LMNG), 0.025% cholesteryl hemisuccinate (CHS), 50 mM HEPES pH 7.0, and 500 mM NaCl for 5–6 hours followed by ultracentrifugation at 200,000 × g for 30 minutes to remove unsolubilized material. Co^{2+}-charged affinity resin (Talon, Clontech) and imidazole (30 mM final concentration), were added to the supernatant and incubated overnight at 4 °C. Resin was washed with 20 column volumes wash buffer 1 (25 mM HEPES pH 7.0, 500 mM NaCl, 10 mM $MgCl_2$, 0.1% LMNG, 0.005% CHS, 8 mM ATP, 30 mM imidazole), 2 times 20 column volumes wash buffer 2 (25 mM HEPES pH 7.0, 250 mM NaCl, 0.05% LMNG, 0.0025% CHS, 5% glycerol, 30 mM imidazole and ligand), and eluted with buffer 3 (25 mM HEPES pH 7.0, 250 mM NaCl, 0.05% LMNG, 0.0025% CHS, 5% glycerol, 300 mM imidazole and ligand). After elution, samples were exchanged into NMR buffer (20 mM HEPES pH 7.0, 75 mM NaCl, 0.025% LMNG, 0.00125% CHS, and ligand), using a PD-10 desalting column (G.E. Healthcare). All buffers were prepared with ligand at saturating concentration. Samples were concentrated to 280 μL in a Vivaspin-6 concentrator with a 30 kDa MWCO (Sartorius) and 20 μL D_2O was added prior to transferring to a 5 mm Shigemi NMR tube. All samples were purified in protonated buffers containing the antagonist theophylline. Theophylline was exchanged with other ligands during the protein purification.

NMR Spectroscopy—2-dimensional [^{15}N,^{1}H]-transverse relaxation-optimized spectroscopy (TROSY) (Pervushin et al., 1997) correlation spectra were measured on a Bruker Avance 800 MHz spectrometer equipped with a 5-mm TXI-HCN probe running Topspin 3.1 (Bruker Biospin). Experiments were measured at 307 Kelvin. The sample temperature was calibrated using a standard sample (4% methanol in methanol-d4). Chemical shifts were referenced to an internal DSS standard. TROSY spectra were typically recorded with acquisition periods of 98 ms in ^{1}H and 22.5 ms in ^{15}N, with a 1 s recycle delay for a total experimental time of about 18 hours per experiment. NMR data were processed and analyzed in Topspin 3.5pl2 (Bruker Biospin). All data were processed identically; prior to Fourier transformation, the data matrices were zero filled to 1024 (t1) × 4096 (t2) complex points and multiplied by a Gaussian window function in the acquisition dimension and a 75°-shifted sine bell window function in the indirect dimension.

Radioligand Binding Assays in Membranes—Radioligand binding assays were performed using membranes prepared from *Pichia pastoris* expressing WT human A_{2A}AR or one of the variant proteins. For saturation binding experiments, increasing concentrations (ranging from 2 nM to 80 nM) of [^{3}H]2-[p-(2-carboxyethyl)phenyl-ethylamino]-5′-*N*-ethylcarboxamidoadenosine ([^{3}H]CGS21680, 35.2 Ci/mmol) or increasing concentrations of [^{3}H]4-[2-[7-amino-2-(2-furyl)-1,2,4-triazolo[1,5-a][1,3,5]triazin-5-yl-amino]ethylphenol ([^{3}H]ZM241385, 0.2 nM to 12 nM) were incubated with membranes (5 μg protein) at 25°C for 60 min in a total of 200 μl Tris–HCl buffer (50 mM, pH 7.5) containing 10 mM $MgCl_2$. Adenosine-5′-*N*-ethyluronamide (NECA, 100 μM) or 8-[4-[[[[(2-aminoethyl)amino]carbonyl]methyl)oxy]phenyl]-1,3-dipropylxanthine (XAC, 10 μM) was used to determine the non-specific binding. For displacement binding experiments, increasing concentrations of ligands were incubated with [^{3}H]CGS21680 (5 nM) and membrane preparations at 25 °C for 60 min. Binding reactions were terminated by filtration through Whatman GF/B filters under reduced pressure using an MT-24 cell harvester (Brandell, Gaithersburg, MD, USA) and followed by washing twice with 5 ml cold Tris-HCl buffer. Radioactivity was measured using a scintillation counter (Tri-Carb 2810TR).

Radioligand Binding Assays for A_{2A}AR Reconstituted in LMNG/CHS Micelles—Radioligand binding assays were performed using a scintillation proximity assay previously described (Bocquet et al., 2015). Ligand binding was measured using purified A_{2A}AR reconstituted in LMNG/CHS micelles. Binding assays were carried out in a total volume of 175 μl per well in 96-well plates with binding buffer (150 mM NaCl, 0.05% LMNG, 0.0025% CHS, 25 mM HEPES, pH 7.0) containing approximately 0.05 μg A_{2A}AR, 1nM [^{3}H] ZM241385 (American Radiolabelled Chemicals, Inc.), a dose range of competing compound (10^{-12} – 10^{-5}, M), and 250 μg of YSi copper His-tag SPA beads (Perkin Elmer), which were incubated for 60 min at 4 °C on a shaker. [^{3}H] ZM241385 (25 μL) and competing compound (25 μL) were added to the 96-well plates first followed by A_{2A}AR (25 μL) and SPA beads (100 μL). Binding was detected in a MicroBeta2 TriLux plate scintillation counter (Perkin Elmer) using SPA mode. ZM241385 binding affinity (K_D) was determined using homologous competition binding, and competition binding assays were done to determine K_i values for NECA, XAC, and CGS21680. Controls were done to optimize the ratio of SPA beads to protein to minimize non-specific binding and ensure no more than 10% of free ligand was bound.

A_{2A}AR Crystallization, Data Collection, Structure Calculation and Refinement—A_{2A}AR-BRIL in complex with ZM241385 was reconstituted into lipidic cubic phase (LCP) by previously reported methods (Caffrey and Cherezov, 2009). Diffraction quality crystals were obtained with the same conditions as used for the crystallization of *Sf9*-produced A_{2A}AR-BRIL(Chun et al., 2012; Liu et al., 2012b).

X-ray diffraction data were collected on the 23ID-D beamline (GM/CA CAT) at the Advanced Photon Source, Argonne, IL using a Pilatus3 6M detector (X-ray wavelength 1.033 Å). The crystals were exposed with a 10 μm mini-beam for 1 second and 1.0° oscillation per frame. HKL2000 (Otwinowski and Minor, 1997) was used for integrating,

scaling and merging data from 18 best-diffracting crystals of the A_{2A}AR–BRIL from *Pichia pastoris* in complex with ZM241385.

Initial phase information of A_{2A}AR–BRIL from *Pichia pastoris* was obtained by molecular replacement (MR) with PHASER (McCoy et al., 2007) using A_{2A}AR–BRIL (PDB: 4EIY) as a search model. Refinement was performed with REFMAC5 (Murshudov et al., 1997; Otwinowski and Minor, 1997) and autoBUSTER (Bricogne G., 2016) followed by manual examination and rebuilding of the refined coordinates in the program COOT (Emsley and Cowtan, 2004), using both $|2F_o|-|F_c|$ and $|F_o| - |F_c|$ maps. TLS refinement strategy with two TLS groups (GPCR and BRIL domains) was incorporated in the refinement.

The final model of the A_{2A}AR–BRIL complex contains residues −2 to −1 from the expression tag, 1–208, 219–306 of A_{2A}AR, 1001–1042 and 1058–1106 of BRIL, and the ligand ZM241385 (ZMA as defined in the coordinate file), 3 cholesterols, 7 oleic acids, 5 OLC (or OLB), and 15 waters. The remaining C-terminal residues beyond 306 were disordered and not visible in the electron density maps and were therefore not modelled. The final model has good stereochemistry with no Ramachandran outliers (98.7% in favored and 1.3% in allowed regions), as determined by Molprobity (Chen et al., 2010). Data collection and refinement statistics are summarized in Table S3.

Quantification and Statistical Analysis

Quantification and analysis of ligand binding for A_{2A}AR in *Pichia* membranes: Binding parameters were calculated using Prism 6 software (GraphPad). IC_{50} values obtained from displacement curves were converted to K_i values using the Cheng–Prusoff equation (Yung-Chi and Prusoff, 1973). All data are expressed as the mean ± standard error from three independent experiments performed in triplicate.

Quantification of ligand binding for A_{2A}AR in LMNG/CHS performed by the scintillation proximity assay: The data were analyzed by Prism 6.05 (GraphPad) to give K_D and K_i values and reported as the mean ± S.D. and done three times or more in triplicate.

Data and Software Availability—NMR assignments have been deposited in the Biological Magnetic Resonance Data Bank (BMRB) with Entry ID … The structure of A_{2A}AR-BRIL in complex with ZM241385 expressed in *P. pastoris* has been deposited in the Protein Data Bank (PDB) with the ID PDB 6QAF.

Supplementary Material

Refer to Web version on PubMed Central for supplementary material.

Acknowledgments

The authors acknowledge support from NIH/NIGMS PSI: Biology grant U54 GM094618 and R01GM115825, and from the NIDDK Intramural Research Program. M.T.E. acknowledges funding from an American Cancer Society postdoctoral fellowship. K.W. is the Cecil H. and Ida M. Green Professor of Structural Biology at The Scripps Research Institute. The authors thank Sophie Nguyen for help with the production of A_{2A}AR biomass, Jeffrey Velasquez for help in cloning of A_{2A}AR constructs, Yekaterina Kadyshevskaya for help with the preparation of figures, Dr. Vsevold Katritch for input on the manuscript, and Angela Walker for careful checking of the manuscript.

References

Audet M, Bouvier M. Restructuring G-Protein-Coupled Receptor Activation. Cell. 2012; 151:14–23. [PubMed: 23021212]

Ballesteros JA, Weinstein H. Integrated methods for the construction of three-dimensional models and computational probing of structure-function relations in G protein-coupled receptors. Methods Neurosi. 1995; 25:366–428.

Bara-Jimenez W, Sherzai A, Dimitrova T, Favit A, Bibbiani F, Gillespie M, Morris M, Mouradian M, Chase T. Adenosine A2A receptor antagonist treatment of Parkinson's disease. Neurology. 2003; 61:293–296. [PubMed: 12913186]

Beck M, Sakmar TP, Siebert F. Spectroscopic evidence for interaction between transmembrane helices 3 and 5 in rhodopsin. Biochemistry. 1998; 37:7630–7639. [PubMed: 9585578]

Bihoreau C, Monnot C, Davies E, Teutsch B, Bernstein KE, Corvol P, Clauser E. Mutation of Asp74 of the rat angiotensin II receptor confers changes in antagonist affinities and abolishes G-protein coupling. Proc Natl Acad Sci USA. 1993; 90:5133–5137. [PubMed: 8506360]

Bocquet N, Kohler J, Hug MN, Kusznir EA, Rufer AC, Dawson RJ, Hennig M, Ruf A, Huber W, Huber S. Real-time monitoring of binding events on a thermostabilized human A2A receptor embedded in a lipid bilayer by surface plasmon resonance. BBA - Biomembranes. 2015; 1848:1224–1233. [PubMed: 25725488]

Bokoch MP, Zou Y, Rasmussen SGF, Liu CW, Nygaard R, Rosenbaum DM, Fung JJ, Choi HJ, Thian FS, Kobilka TS, et al. Ligand-specific regulation of the extracellular surface of a G-protein-coupled receptor. Nature. 2010; 463:108–112. [PubMed: 20054398]

Bricogne, G., BE, Brandl, M., Flensburg, C., Keller, P., Paciorek, W., Roversi, P., Sharff, A., Smart, OS., Vonrhein, C., Womack, TO. BUSTER version 2.10.1. Cambridge, United Kingdom: Global Phasing Ltd; 2016.

Caffrey M, Cherezov V. Crystallizing membrane proteins using lipidic mesophases. Nat Protoc. 2009; 4:706–731. [PubMed: 19390528]

Carpenter B, Nehmé R, Warne T, Leslie AGW, Tate CG. Structure of the adenosine A(2A) receptor bound to an engineered G protein. Nature. 2016; 536:104–107. [PubMed: 27462812]

Chen VB, Arendall WB, Headd JJ, Keedy DA, Immormino RM, Kapral GJ, Murray LW, Richardson JS, Richardson DC. MolProbity: all-atom structure validation for macromolecular crystallography. Acta Crystallographica Section D: Biological Crystallography. 2010; 66:12–21. [PubMed: 20057044]

Cheng RKY, Segala E, Robertson N, Deflorian F, Doré AS, Errey JC, Fiez-Vandal C, Marshall FH, Cooke RM. Structures of Human A1 and A2A Adenosine Receptors with Xanthines Reveal Determinants of Selectivity. Structure. 2017; 25:1275–1285. e1274. [PubMed: 28712806]

Chun E, Thompson AA, Liu W, Roth CB, Griffith MT, Katritch V, Kunken J, Xu F, Cherezov V, Hanson MA, et al. Fusion Partner Toolchest for the Stabilization and Crystallization of G Protein-Coupled Receptors. Structure/Folding and Design. 2012; 20:967–976. [PubMed: 22681902]

Chung KY, Kim TH, Manglik A, Alvares R, Kobilka BK, Prosser RS. Role of Detergents in Conformational Exchange of a G Protein-coupled Receptor. J Biol Chem. 2012; 287:36305–36311. [PubMed: 22893704]

Cooper DM, Londos C, Gill DL, Rodbell M. Opiate Receptor-Mediated Inhibition of Adenylate Cyclase in Rat Striatal Plasma Membranes. J Neurochem. 1982; 38:1164–1167. [PubMed: 6278084]

Crocker E, Eilers M, Ahuja S, Hornak V, Hirshfeld A, Sheves M, Smith SO. Location of Trp265 in metarhodopsin II: implications for the activation mechanism of the visual receptor rhodopsin. J Mol Biol. 2006; 357:163–172. [PubMed: 16414074]

DeVree BT, Mahoney JP, Vélez-Ruiz GA, Rasmussen SGF, Kuszak AJ, Edwald E, Fung JJ, Manglik A, Masureel M, Du Y, et al. Allosteric coupling from G protein to the agonist-binding pocket in GPCRs. Nature. 2016; 535:182–186. [PubMed: 27362234]

Didenko T, Liu JJ, Horst R, Stevens RC, Wüthrich K. Fluorine-19 NMR of integral membrane proteins illustrated with studies of GPCRs. Curr Opin Struct Biol. 2013; 23:740–747. [PubMed: 23932201]

Doré AS, Robertson N, Errey JC, Ng I, Hollenstein K, Tehan B, Hurrell E, Bennett K, Congreve M, Magnani F, et al. Structure of the Adenosine A2A Receptor in Complex with ZM241385 and the Xanthines XAC and Caffeine. Structure. 2011; 19:1283–1293. [PubMed: 21885291]

Dunwiddie TV, Masino SA. The role and regulation of adenosine in the central nervous system. Annu Rev Neurosci. 2001; 24:31–55. [PubMed: 11283304]

Eddy MT, Didenko T, Stevens RC, Wüthrich K. β2-Adrenergic Receptor Conformational Response to Fusion Protein in the Third Intracellular Loop. Structure. 2016; 24:2190–2197. [PubMed: 27839952]

Elling CE, Frimurer TM, Gerlach L-O, Jorgensen R, Holst B, Schwartz TW. Metal ion site engineering indicates a global toggle switch model for seven-transmembrane receptor activation. J Biol Chem. 2006; 281:17337–17346. [PubMed: 16567806]

Emsley P, Cowtan K. Coot: model-building tools for molecular graphics. Acta Crystallographica Section D: Biological Crystallography. 2004; 60:2126–2132. [PubMed: 15572765]

Fahmy K, Siebert F, Sakmar TP. Photoactivated state of rhodopsin and how it can form. Biophys Chem. 1995; 56:171–181. [PubMed: 7662864]

Fenalti G, Giguere PM, Katritch V, Huang XP, Thompson AA, Cherezov V, Roth BL, Stevens RC. Molecular control of d-opioid receptor signalling. Nature. 2014; 506:191–196. [PubMed: 24413399]

Franke RR, König B, Sakmar TP, Khorana HG, Hofmann KP. Rhodopsin mutants that bind but fail to activate transducin. Science. 1990; 250:123–125. [PubMed: 2218504]

Han M, Smith SO, Sakmar TP. Constitutive Activation of Opsin by Mutation of Methionine 257 on Transmembrane Helix 6. Biochemistry. 1998; 37:8253–8261. [PubMed: 9609722]

Horst R, Liu JJ, Stevens RC, Wüthrich K. β_2-adrenergic receptor activation by agonists studied with ^{19}F NMR spectroscopy. Angew Chem Int Ed Engl. 2013; 52:10762–10765. [PubMed: 23956158]

Hua T, Vemuri K, Nikas SP, Laprairie RB, Wu Y, Qu L, Pu M, Korde A, Jiang S, Ho JH, et al. Crystal structures of agonist-bound human cannabinoid receptor CB1. Nature. 2017; 547:468–471. [PubMed: 28678776]

Isogai S, Deupi X, Opitz C, Heydenreich FM, Tsai CJ, Brueckner F, Schertler GF, Veprintsev DB, Grzesiek S. Backbone NMR reveals allosteric signal transduction networks in the β1-adrenergic receptor. Nature. 2016; 530:237–241. [PubMed: 26840483]

Jaakola VP, Griffith MT, Hanson MA, Cherezov V, Chien EYT, Lane JR, IJzerman AP, Stevens RC. The 2.6 angstrom crystal structure of a human A2A adenosine receptor bound to an antagonist. Science. 2008; 322:1211–1217. [PubMed: 18832607]

Johnson C Jr, Bovey F. Calculation of nuclear magnetic resonance spectra of aromatic hydrocarbons. J Chem Phys. 1958; 29:1012–1014.

Katritch V, Cherezov V, Stevens RC. Diversity and modularity of G protein-coupled receptor structures. Trends Pharmacol Sci. 2012; 33:17–27. [PubMed: 22032986]

Katritch V, Fenalti G, Abola EE, Roth BL, Cherezov V, Stevens RC. Allosteric sodium in class A GPCR signaling. Trends Biochem Sci. 2014; 39:233–244. [PubMed: 24767681]

Kim TH, Chung KY, Manglik A, Hansen AL, Dror RO, Mildorf TJ, Shaw DE, Kobilka BK, Prosser RS. The role of ligands on the equilibria between functional states of a G protein-coupled receptor. J Am Chem Soc. 2013; 135:9465–9474. [PubMed: 23721409]

Kimata N, Pope A, Eilers M, Opefi CA, Ziliox M, Hirshfeld A, Zaitseva E, Vogel R, Sheves M, Reeves PJ. Retinal orientation and interactions in rhodopsin reveal a two-stage trigger mechanism for activation. Nature Comm. 2016; 7:12683.

Klein-Seetharaman J, Getmanova EV, Loewen MC, Reeves PJ, Khorana HG. NMR spectroscopy in studies of light-induced structural changes in mammalian rhodopsin: Applicability of solution 19F NMR. Proc Natl Acad Sci USA. 1999; 96:13744–13749. [PubMed: 10570143]

Kofuku Y, Ueda T, Okude J, Shiraishi Y, Kondo K, Maeda M, Tsujishita H, Shimada I. Efficacy of the β2-adrenergic receptor is determined by conformational equilibrium in the transmembrane region. Nature Comm. 2012; 3:1045.

Kofuku Y, Ueda T, Okude J, Shiraishi Y, Kondo K, Mizumura T, Suzuki S, Shimada I. Functional dynamics of deuterated β2-adrenergic receptor in lipid bilayers revealed by NMR spectroscopy. Angew Chem Int Ed Engl. 2014; 53:13376–13379. [PubMed: 25284766]

Koradi R, Billeter M, Wüthrich K. MOLMOL: A program for display and analysis of macromolecular structures. J Mol Graph. 1996; 14:51–55. [PubMed: 8744573]

Lebon G, Warne T, Edwards PC, Bennett K, Langmead CJ, Leslie AGW, Tate CG. Agonist-bound adenosine A2A receptor structures reveal common features of GPCR activation. Nature. 2011; 474:521–525. [PubMed: 21593763]

Lin SW, Han M, Sakmar TP. Analysis of functional microdomains of rhodopsin. Methods Enzymol. 2000; 315:116–130. [PubMed: 10736698]

Lin SW, Sakmar TP. Specific Tryptophan UV-Absorbance Changes Are Probes of the Transition of Rhodopsin to Its Active State. Biochemistry. 1996; 35:11149–11159. [PubMed: 8780519]

Liu D, Wüthrich K. Ring current shifts in 19F-NMR of membrane proteins. J Biomol NMR. 2016; 65:1–5. [PubMed: 27240587]

Liu JJ, Horst R, Katritch V, Stevens RC, Wüthrich K. Biased signaling pathways in β2-adrenergic receptor characterized by 19F-NMR. Science. 2012a; 335:1106–1110. [PubMed: 22267580]

Liu W, Chun E, Thompson AA, Chubukov P, Xu F, Katritch V, Han GW, Roth CB, Heitman LH, IJzerman AP, et al. Structural basis for allosteric regulation of GPCRs by sodium ions. Science. 2012b; 337:232–236. [PubMed: 22798613]

MacDonald C, Phillips W. Manifestations of the Tertiary Structures of Proteins in High-Frequency NMR. J Am Chem Soc. 1967; 89:6332. [PubMed: 6055984]

Manglik A, Kim TH, Masureel M, Altenbach C, Yang Z, Hilger D, Lerch MT, Kobilka TS, Thian FS, Hubbell WL, et al. Structural Insights into the Dynamic Process of β2-Adrenergic Receptor Signaling. Cell. 2015; 161:1101–1111. [PubMed: 25981665]

Manglik A, Kobilka B. The role of protein dynamics in GPCR function: insights from the β2AR and rhodopsin. Curr Opin Cell Biol. 2014; 27:136–143. [PubMed: 24534489]

Markley JL, Putter I, Jardetzky O. High-resolution nuclear magnetic resonance spectra of selectively deuterated staphylococcal nuclease. Science. 1968; 161:1249–1251. [PubMed: 5673435]

Martin S, Botto JM, Vincent JP, Mazella J. Pivotal role of an aspartate residue in sodium sensitivity and coupling to G proteins of neurotensin receptors. Mol Pharmacol. 1999; 55:210–215. [PubMed: 9927610]

Massink A, Gutierrez-de-Teran H, Lenselink EB, Ortiz Zacarias NV, Xia L, Heitman LH, Katritch V, Stevens RC, Jzerman IAP. Sodium Ion Binding Pocket Mutations and Adenosine A2A Receptor Function. Mol Pharmacol. 2014; 87:305–313. [PubMed: 25473121]

McCoy AJ, Grosse-Kunstleve RW, Adams PD, Winn MD, Storoni LC, Read RJ. Phaser crystallographic software. Journal of applied crystallography. 2007; 40:658–674. [PubMed: 19461840]

Munk C, Isberg V, Mordalski S, Harpsøe K, Rataj K, Hauser A, Kolb P, Bojarski A, Vriend G, Gloriam D. GPCRdb: the G protein-coupled receptor database–an introduction. Br J Pharmacol. 2016

Murshudov GN, Vagin AA, Dodson EJ. Refinement of macromolecular structures by the maximum-likelihood method. Acta Crystallographica Section D: Biological Crystallography. 1997; 53:240–255. [PubMed: 15299926]

Nygaard R, Zou Y, Dror RO, Mildorf TJ, Arlow DH, Manglik A, Pan AC, Liu CW, Fung JJ, Bokoch MP, et al. The dynamic process of β2-adrenergic receptor activation. Cell. 2013; 152:532–542. [PubMed: 23374348]

Ohta A, Sitkovsky M. Role of G-protein-coupled adenosine receptors in downregulation of inflammation and protection from tissue damage. Nature. 2001; 414:916–920. [PubMed: 11780065]

Okude J, Ueda T, Kofuku Y, Sato M, Nobuyama N, Kondo K, Shiraishi Y, Mizumura T, Onishi K, Natsume M, et al. Identification of a Conformational Equilibrium That Determines the Efficacy and Functional Selectivity of the μ-Opioid Receptor. Angew Chem Int Ed Engl. 2015; 54:15771–15776. [PubMed: 26568421]

Otwinowski Z, Minor W. Processing of X-ray diffraction data collected in oscillation mode. Methods Enzymol. 1997; 276:307–326.

Palmer TM, Stiles GL. Identification of an A2a adenosine receptor domain specifically responsible for mediating short-term desensitization. Biochemistry. 1997; 36:832–838. [PubMed: 9020781]

Perkins SJ, Wüthrich K. Ring current effects in the conformation dependent NMR chemical shifts of aliphatic protons in the basic pancreatic trypsin inhibitor. Biochim Biophys Acta. 1979; 576:409–423. [PubMed: 427198]

Pert CB, Pasternak G, Snyder SH. Opiate agonists and antagonists discriminated by receptor binding in brain. Science and Psychiatry: Groundbreaking Discoveries in Molecular Neuroscience. 2009:19.

Pervushin K, Riek R, Wider G, Wüthrich K. Attenuated T2 relaxation by mutual cancellation of dipole-dipole coupling and chemical shift anisotropy indicates an avenue to NMR structures of very large biological macromolecules in solution. Proc Natl Acad Sci USA. 1997; 94:12366–12371. [PubMed: 9356455]

Rasmussen SG, DeVree BT, Zou Y, Kruse AC, Chung KY, Kobilka TS, Thian FS, Chae PS, Pardon E, Calinski D. Crystal structure of the β2 adrenergic receptor-Gs protein complex. Nature. 2011; 477:549–555. [PubMed: 21772288]

Rosenbaum DM, Rasmussen SGF, Kobilka BK. The structure and function of G-protein-coupled receptors. Nature. 2009; 459:356–363. [PubMed: 19458711]

Sakmar TP, Fahmy K. Properties and Photoactivity of Rhodopsin Mutants. Isr J Chem. 1995; 35:325–337.

Schwartz TW, Frimurer TM, Holst B, Rosenkilde MM, Elling CE. Molecular Mechanism of 7TM Receptor Activation—A Global Toggle Switch Model. Annu Rev Pharmacol Toxicol. 2006; 46:481–519. [PubMed: 16402913]

Segala E, Guo D, Cheng RKY, Bortolato A, Deflorian F, Doré AS, Errey JC, Heitman LH, Jzerman IAP, Marshall FH, et al. Controlling the Dissociation of Ligands from the Adenosine A 2AReceptor through Modulation of Salt Bridge Strength. J Med Chem. 2016; 59:6470–6479. [PubMed: 27312113]

Shi L, Liapakis G, Xu R, Guarnieri F, Ballesteros JA, Javitch JA. Beta2 adrenergic receptor activation. Modulation of the proline kink in transmembrane 6 by a rotamer toggle switch. J Biol Chem. 2002; 277:40989–40996. [PubMed: 12167654]

Shieh T, Han M, Sakmar TP, Smith SO. The steric trigger in rhodopsin activation. J Mol Biol. 1997; 269:373–384. [PubMed: 9199406]

Sounier R, Mas C, Steyaert J, Laeremans T, Manglik A, Huang W, Kobilka BK, Déméné H, Granier S. Propagation of conformational changes during μ-opioid receptor activation. Nature. 2015; 524:375–378. [PubMed: 26245377]

Staus DP, Strachan RT, Manglik A, Pani B, Kahsai AW, Kim TH, Wingler LM, Ahn S, Chatterjee A, Masoudi A, et al. Allosteric nanobodies reveal the dynamic range and diverse mechanisms of G-protein-coupled receptor activation. Nature. 2016; 535:448–452. [PubMed: 27409812]

Steen A, Thiele S, Guo D, Hansen LS, Frimurer TM, Rosenkilde MM. Biased and constitutive signaling in the CC-chemokine receptor CCR5 by manipulating the interface between transmembrane helices 6 and 7. J Biol Chem. 2013; 288:12511–12521. [PubMed: 23493400]

Sun B, Bachhawat P, Chu MLH, Wood M, Ceska T, Sands ZA, Mercier J, Lebon F, Kobilka TS, Kobilka BK. Crystal structure of the adenosine A 2Areceptor bound to an antagonist reveals a potential allosteric pocket. Proc Natl Acad Sci USA. 2017; 114:2066–2071. [PubMed: 28167788]

Tao Q, Abood ME. Mutation of a highly conserved aspartate residue in the second transmembrane domain of the cannabinoid receptors, CB1 and CB2, disrupts G-protein coupling. J Pharmacol Exp Ther. 1998; 285:651–658. [PubMed: 9580609]

Venkatakrishnan AJ, Deupi X, Lebon G, Heydenreich FM, Flock T, Miljus T, Balaji S, Bouvier M, Veprintsev DB, Tate CG, et al. Diverse activation pathways in class A GPCRs converge near the G-protein-coupling region. Nature. 2016; 536:484–487. [PubMed: 27525504]

Wacker D, Wang C, Katritch V, Han GW, Huang XP, Vardy E, McCorvy JD, Jiang Y, Chu M, Siu FY, et al. Structural features for functional selectivity at serotonin receptors. Science. 2013; 340:615–619. [PubMed: 23519215]

Wüthrich K. High-resolution proton nuclear magnetic resonance spectroscopy of cytochrome c. Proc Natl Acad Sci USA. 1969; 63:1071–1078. [PubMed: 5260911]

Wüthrich, K. NMR of Proteins and Nucleic Acids. John Wiley & Sons; 1986.

Xu F, Wu H, Katritch V, Han GW, Jacobson KA, Gao ZG, Cherezov V, Stevens RC. Structure of an agonist-bound human A2A adenosine receptor. Science. 2011; 332:322–327. [PubMed: 21393508]

Ye L, Van Eps N, Zimmer M, Ernst OP, Prosser RS. Activation of the A2A adenosine G-protein-coupled receptor by conformational selection. Nature. 2016; 533:265–268. [PubMed: 27144352]

Young A, Ngiow SF, Barkauskas DS, Sult E, Hay C, Blake SJ, Huang Q, Liu J, Takeda K, Teng MWL, et al. Co-inhibition of CD73 and A2AR Adenosine Signaling Improves Anti-tumor Immune Responses. Cancer Cell. 2016; 30:391–403. [PubMed: 27622332]

Yung-Chi C, Prusoff WH. Relationship between the inhibition constant (Ki) and the concentration of inhibitor which causes 50 per cent inhibition (I50) of an enzymatic reaction. Biochem Pharmacol. 1973; 22:3099–3108. [PubMed: 4202581]

Highlights

- Comprehensive view of GPCR signaling pathways using NMR probes
- Allosteric signaling monitored by NMR probes distributed throughout $A_{2A}AR$
- Function-related conformational polymorphisms at intracellular $A_{2A}AR$ surface
- Strong coupling between allosteric switch and signaling-activation motif

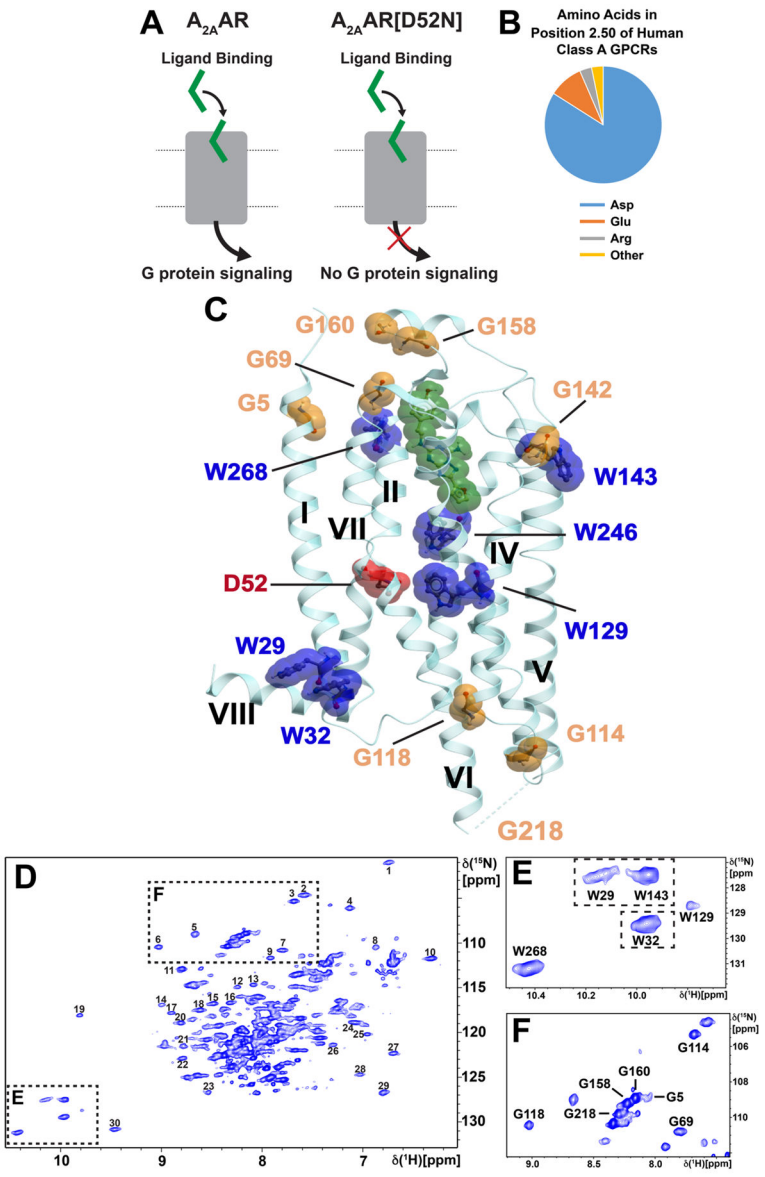

Figure 1. $A_{2A}AR$ Signaling *via* an Allosteric Center at Asp52$^{2.50}$ Probed by an Extensive Network of Assigned NMR Signals

(A) Scheme of agonist-induced signaling in $A_{2A}AR$ and $A_{2A}AR$[D52N], i.e., receptors with and without an active allosteric switch at position 52$^{2.50}$, respectively. The gray shape represents $A_{2A}AR$, the green shape the signal-inducing drug, and the upper and lower thin horizontal lines indicate the extracellular and intracellular membrane surfaces, respectively. (B) Pie chart showing the frequency of amino acid types occurring at position 52$^{2.50}$ in all class A GPCRs: Asp 84%, Glu 10%, Arg and others 6% (Munk et al., 2016). (C) Ribbon representation of the crystal structure of the antagonist ZM241385 (green) complex of $A_{2A}AR$ expressed in *Pichia pastoris* (PDB 6AQF). The location of the fusion protein BRIL in the intracellular loop 3 (ICL3), where G218 was eliminated in the fusion protein, is indicated by a thin broken line; G218 was left intact in the $A_{2A}AR$ sequence used for NMR studies (see Figure S1 for the location of G218 at the intracellular tip of trans-membrane

helix VI in a structure without fusion protein). NMR-assigned tryptophan residues and their sequence positions are highlighted in blue, assigned glycine residues are orange, and the residue Asp52$^{2.50}$ is shown in red. (D) 2D [^{15}N,^{1}H]-TROSY correlation spectrum of A_{2A}AR in complex with ZM241385. Dashed boxes highlight the Trp indole ^{15}N–^{1}H and Gly backbone ^{15}N–^{1}H regions, which are shown on expanded scales in (E) and (F), respectively, with sequence-specific assignments indicated next to the signals. The peaks numbered 1 to 30 were used to monitor the global folds of the A_{2A}AR variants used here for resonance assignments and function-related studies.

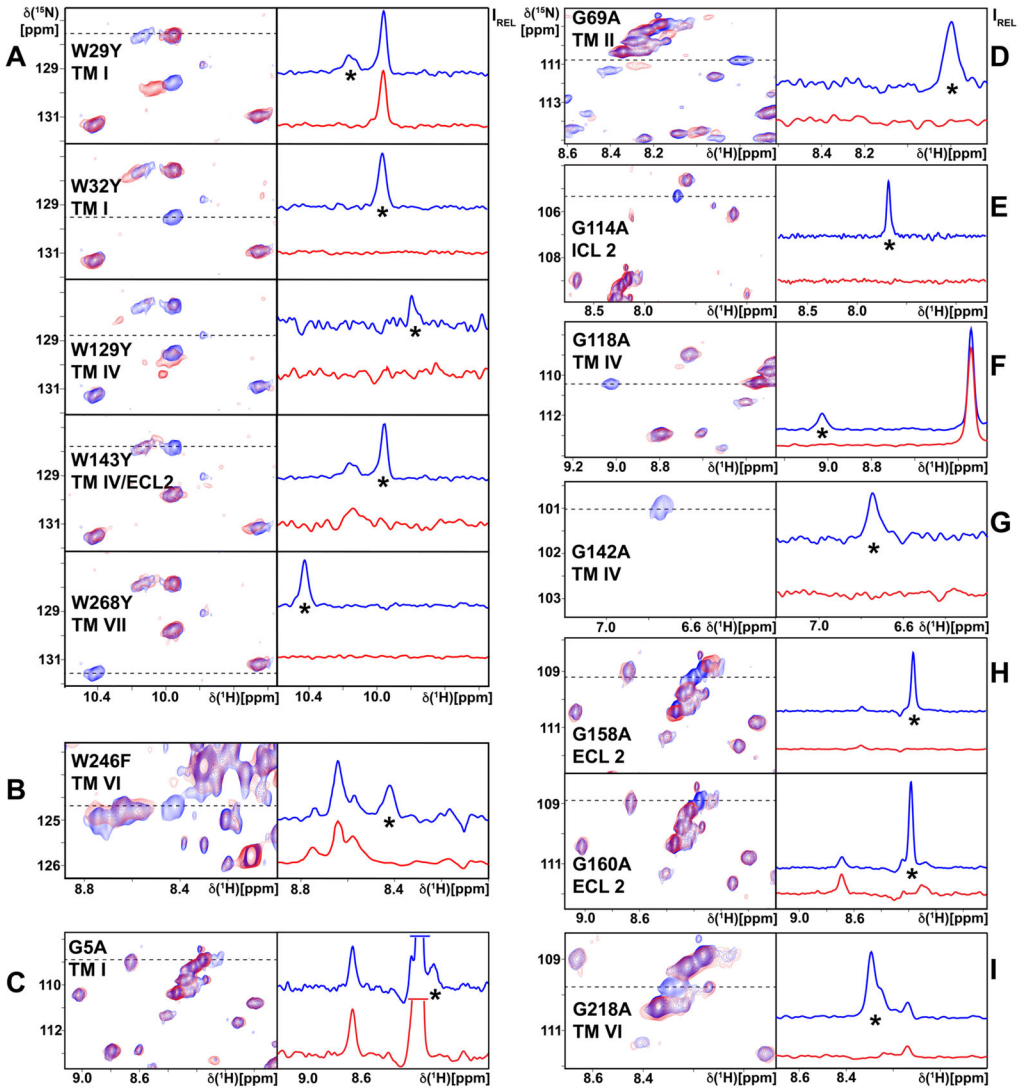

Figure 2. Sequence-specific Assignment of the Trp Indole ^{15}N–^{1}H and Eight Gly Backbone ^{15}N–^{1}H NMR Lines

Panels A and B document the assignments for the tryptophans, and the panels C to I those of eight glycines. Each panel displays a region of the 2D [^{15}N,^{1}H]-TROSY correlation spectrum of A_{2A}AR in complex with ZM241385. On the left are contour plots and on the right are 1D cross sections taken at the ^{15}N chemical shifts indicated by dashed lines in the contour plots. The spectrum of A_{2A}AR is shown in blue, and the spectra of the variant proteins used for the assignment of the residues indicated in the individual panels are shown in red; locations in the 3D A_{2A}AR structure are also indicated, where “TM” stands for “trans-membrane helix”, and “ICL” and “ECL”, respectively, for intracellular and extracellular loop. Comparison of the two spectra resulted in sequence-specific assignment of the signal identified by an asterisk, by observation of the absence in the variant protein of the signal to be assigned. In the right panel of (C), the most intense signals have been truncated.

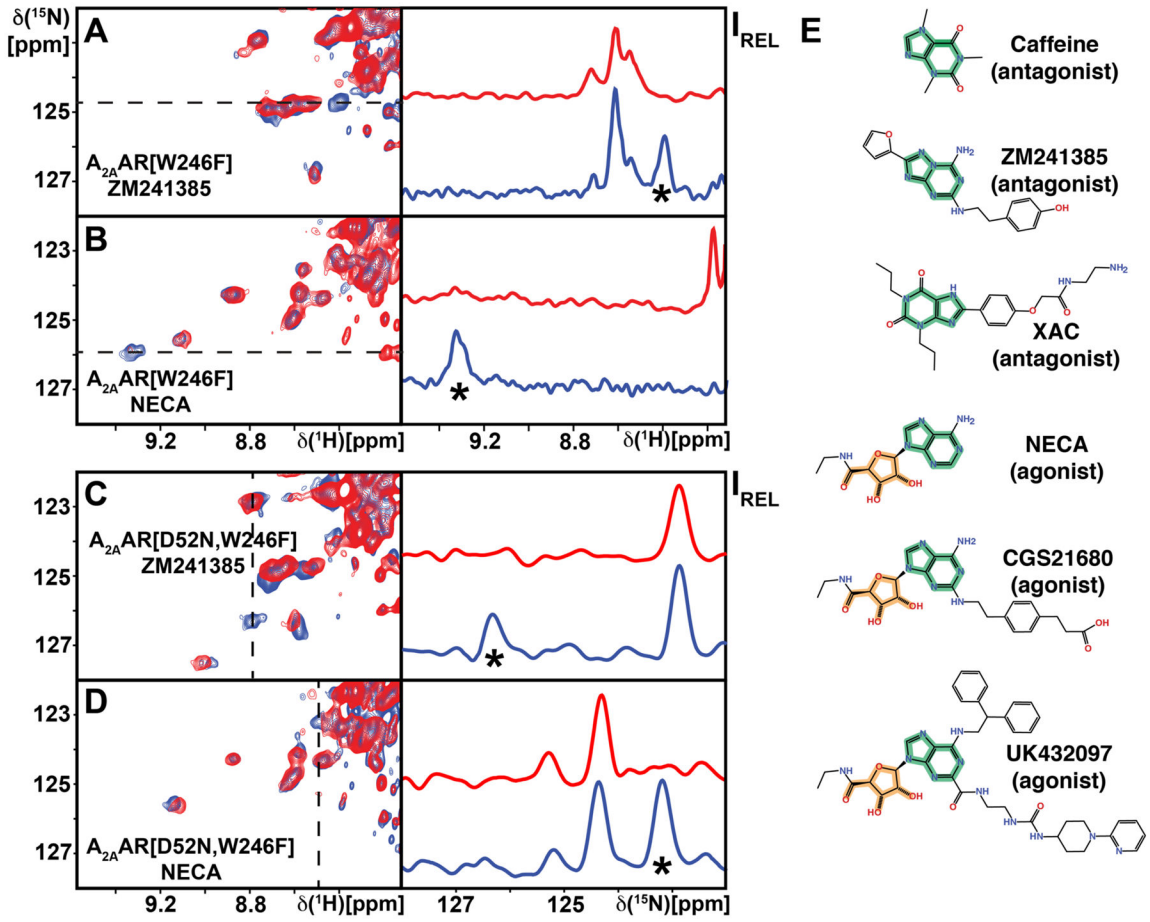

Figure 3. NMR Assignment of the Toggle Switch Trp246$^{6.48}$ in A_{2A}AR and A_{2A}AR[D52N] and Chemical Structures of Ligands Used in this Study

(A and B) Assignment of the Trp246$^{6.48}$ indole ^{15}N–^{1}H signal of A_{2A}AR complexes with different ligands. (A) Antagonist ligand ZM241385. (B) Agonist ligand NECA. (C and D) Corresponding assignments for Trp246$^{6.48}$ in the A_{2A}AR[D52N] complexes with ZM241385 (C) and NECA (D). On the left are contour plots of 2D [^{15}N,^{1}H]-TROSY correlation spectra and on the right are cross sections taken at the ^{15}N or ^{1}H chemical shifts indicated in the contour plots by dashed vertical or horizontal lines, respectively. The spectra of A_{2A}AR and A_{2A}AR[D52N] are shown in blue, and the spectra for the variant proteins used for the resonance assignments are shown in red. Comparison of the two spectra resulted in sequence-specific assignments for the signals identified by asterisks, by observation of the absence in the variant protein of the signal to be assigned. (E) Chemical structures of the ligands used in the current study, where the adenine moiety found in almost all A_{2A}AR antagonists and agonists is highlighted in green, and the ribose moiety found only in A_{2A}AR agonists is highlighted in orange.

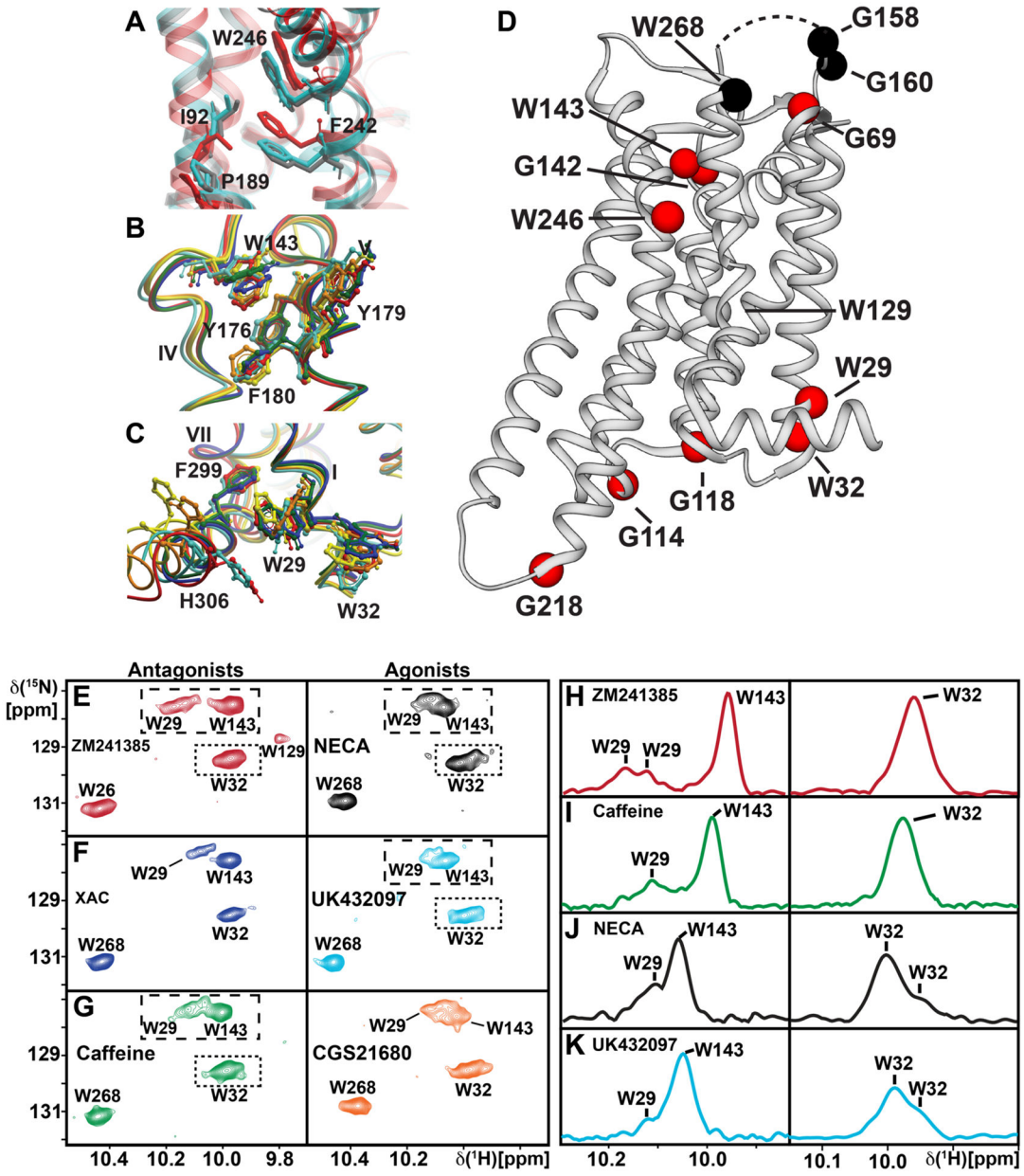

Figure 4. Local Environments of Selected Trp Residues in Crystal Structures of A_{2A}AR and Response of Trp Indole ^{15}N–^{1}H NMR Lines to Variable Efficacy of Bound Drugs

(A) Global superposition of the environment of Trp246$^{6.48}$ in the crystal structures of A_{2A}AR complexes with ZM241385 (red; PDB 3EML) and UK432097 (silver-blue; PDB 3QAK), and the ternary complex with NECA and a “mini-Gs” protein (grey; PDB 5G53). Trp246$^{6.48}$ and the nearby residues F242$^{6.44}$, I92$^{3.40}$ and P189$^{5.50}$ are labeled and shown in stick representation. (B and C) Environment of two Trp residues in the A_{2A}AR complexes with six different ligands (Figure 3E), i.e., ZM241385 (red; PDB 3EML), CGS21680 (orange; PDB 4UHR), UK432097 (silver-blue, PDB 3QAK), NECA (yellow; PDB 2YDV), caffeine (green; PDB 3PWH) and XAC (blue; PDB 3REY). Global superpositions of the crystal structures are shown, with ribbon representations of the backbone and stick

representations of aromatic residues of interest. (B) Trp143. (C) Trp29$^{1.55}$. These structures were used to calculate the ring current shifts in Table S1. (D) Survey of the response of NMR probes in A_{2A}AR to drug efficacy. Assigned Gly and Trp residues are shown as spheres positioned in the structure of the A_{2A}AR-ZM241385 complex (PDB 3PWH). Red spheres indicate that a response was observed, either by different chemical shifts, variation of the signal line shapes, or both. Black spheres indicate that there was no response. The curved dashed line at the top of the receptor indicates the position of ECL2, which was not observed in the crystal structure. (E) – (G) Contour plots of the tryptophan indole ^{15}N–^{1}H region of 2D [^{15}N,^{1}H]-TROSY correlation spectra of [u-^{15}N,~70% ^{2}H]-A_{2A}AR bound to ligands with different efficacies, as identified in each panel. Complexes with antagonists are in the left column and those with agonists on the right. Colors of the spectra correspond to the colors of the corresponding crystal structures of A_{2A}AR–ligand complexes in panels (B) and (C). (H) – (K) Projections of the contents of the boxes in the corresponding contour plots along the ^{15}N chemical shift axis onto the lower boundary of the boxes. The same colors are used as for the contour plots and peak assignments are indicated.

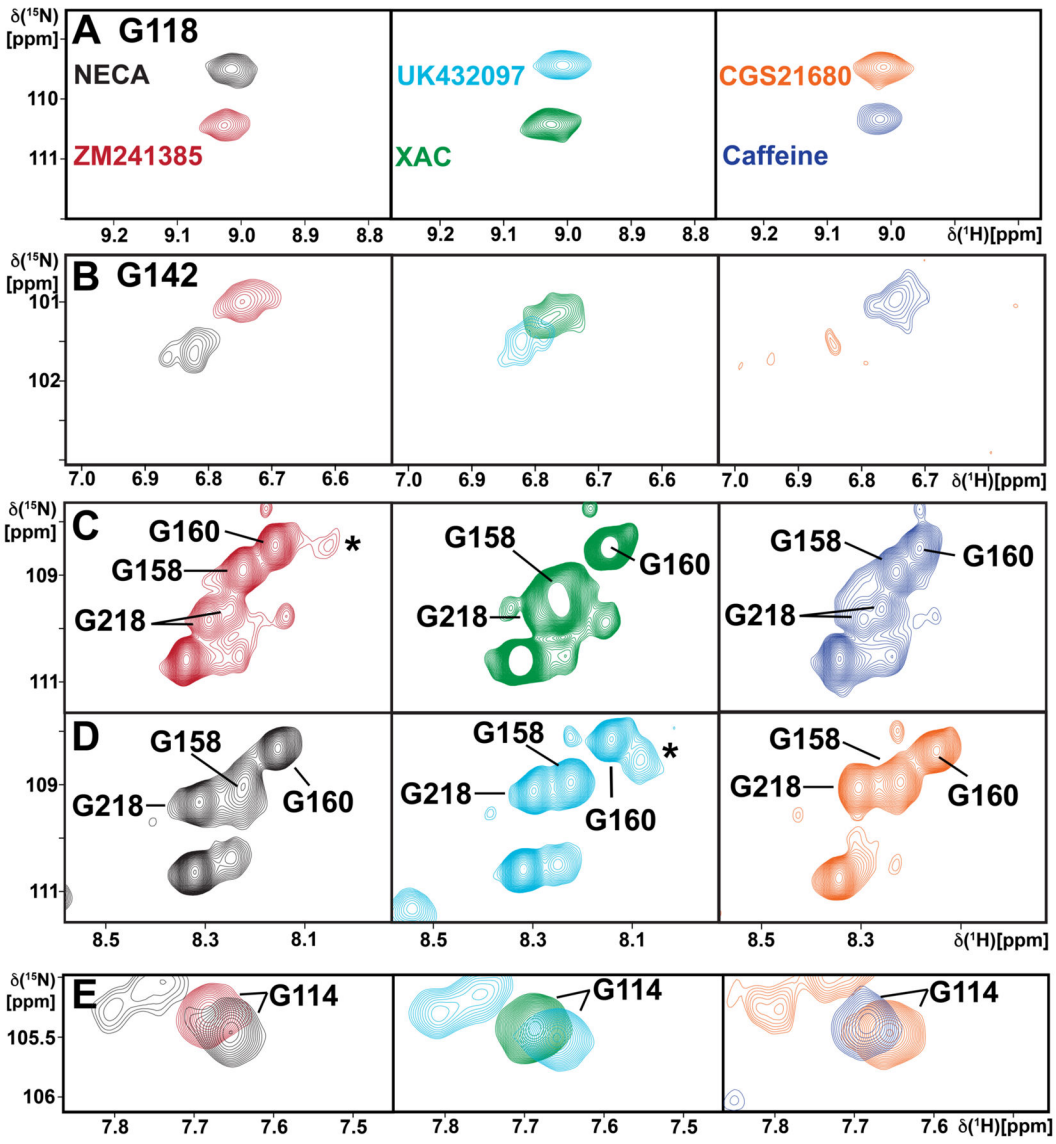

Figure 5. Probing Drug Efficacy-Dependent Signaling in A_{2A}AR by Gly Backbone ^{15}N–^{1}H Resonances

Contour plots are shown of 2D [^{15}N,^{1}H]-TROSY correlation spectra of [u-^{15}N,~70% ^{2}H]-A_{2A}AR complexes with ligands of different efficacies, as identified by the color code in (A) (same colors as in Figure 4B, C, E–G): (A) Gly118$^{4.39}$; (B) Gly142$^{4.63}$; (C and D) Gly158, Gly160 and Gly218; (E) G114. In (A), (B) and (E) each panel shows a superposition of the spectra of complexes with two different ligands, whereas in (C) and (D) each panel displays the spectrum of one complex.

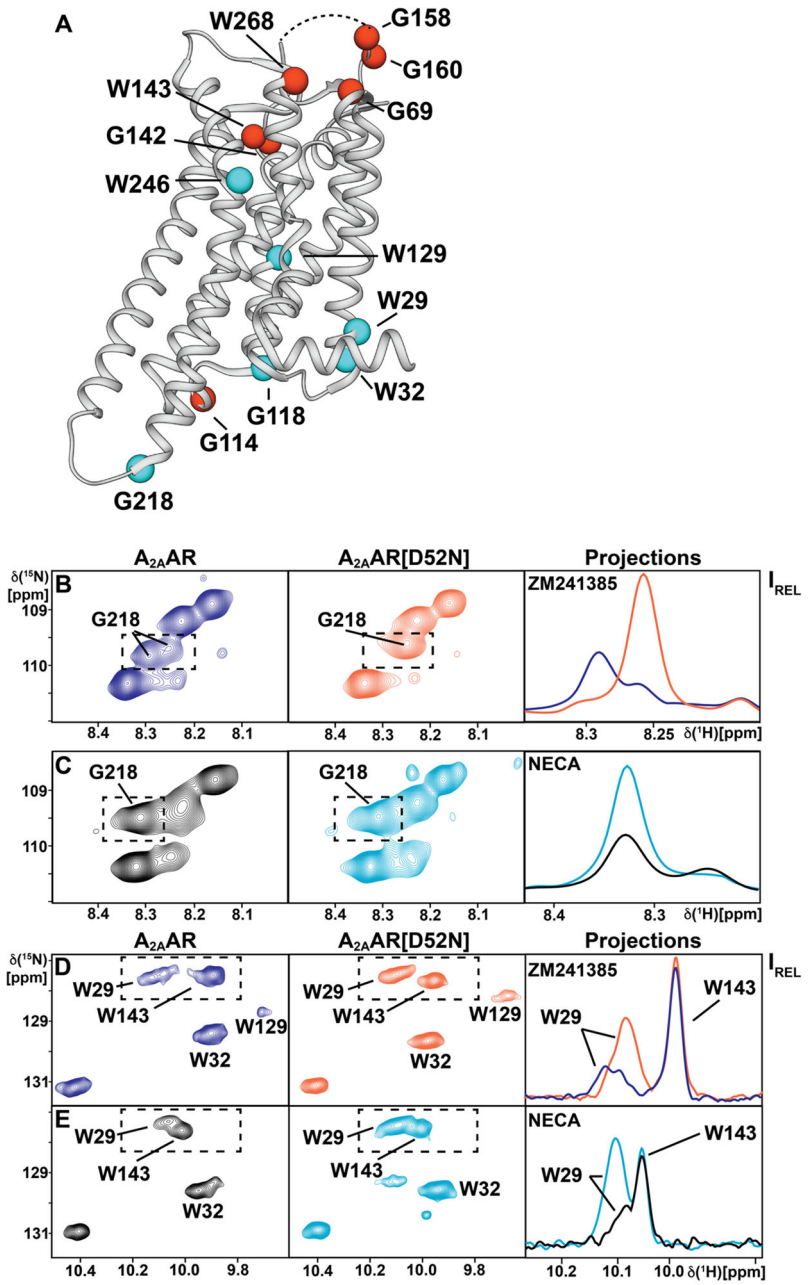

Figure 6. NMR Response on the Extracellular and Intracellular Surfaces of $A_{2A}AR$ to Perturbation of the Allosteric Center at Asp52$^{2.50}$

(A) Survey of the response of NMR Signals in $A_{2A}AR$ to replacement of Asp52$^{2.50}$ in the allosteric center with Asn52$^{2.50}$. Assigned Trp and Gly residues are shown as spheres positioned in the structure of $A_{2A}AR$-ZM241385 (PDB 3PWH). Cyan coloring indicates that changes were observed either in chemical shifts or in NMR line shapes. Red coloring indicates that there was no response. The curved dashed line at the top of the receptor indicates the position of ECL2, which was not observed in the crystal structure. (B)–(E) 2D [^{15}N,^{1}H]-TROSY correlation spectra documenting the results surveyed in (A). On the left and in the center are 2D contour plots, and on the right are projections along the ^{15}N

dimension onto the lower boundary of the regions indicated by the dashed boxes in the contour plots. (B) and (C) Gly218. (D) and (E) Trp29$^{1.55}$, Trp32$^{1.58}$ and Trp143. The proteins and the ligands are identified in the figure; the panels on the right show superpositions of the projections for the two proteins.

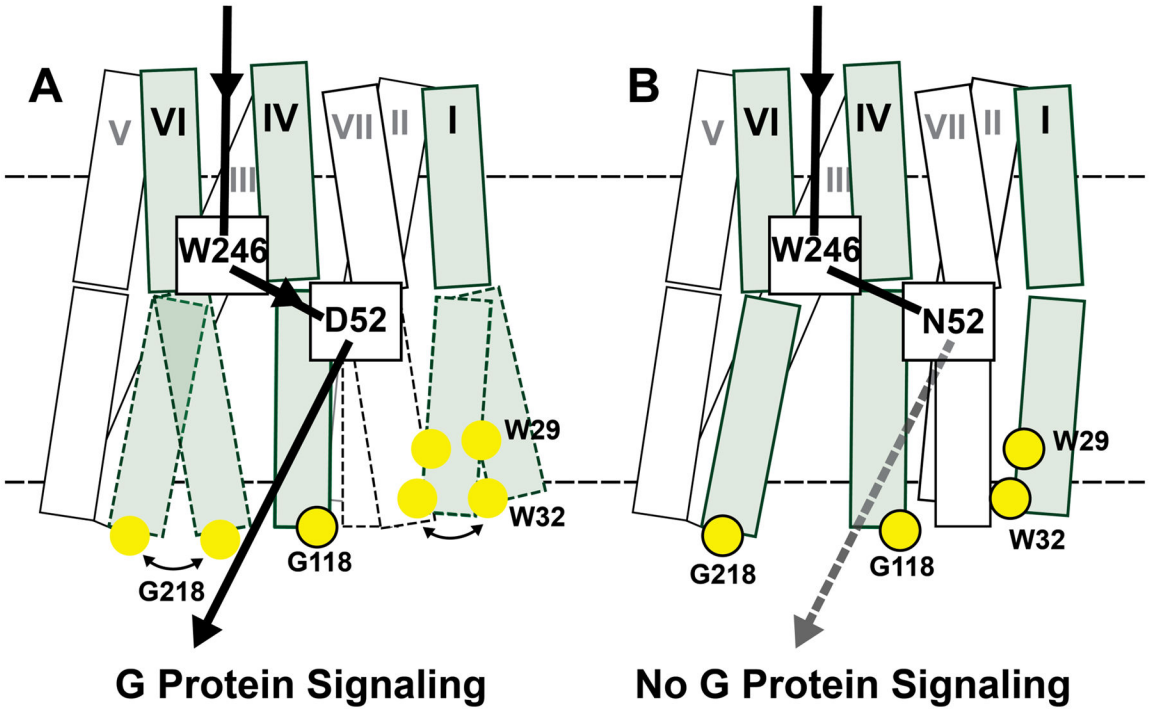

Figure 7. Visualization of Correlations Between Structural and Functional Response to Drug Efficacy and Activity of the Allosteric Center at Asp52$^{2.50}$ in A_{2A}AR

(A) and (B) Schematic side-views of A_{2A}AR and A_{2A}AR[D52N]. The transmembrane helices are represented by two adjoining rectangles, each indicating the extracellular and intracellular subdomains of the receptor (see text). The three helices carrying NMR reporter groups near the intracellular surface are shaded, and the residues with assigned NMR lines are indicated by yellow spheres, where framed spheres indicate that a single NMR line was observed, and unframed spheres correspond to multiple-component resonances. The helices drawn with broken lines indicate the local polymorphisms seen in the NMR spectra of the residues with unframed yellow spheres. The broken horizontal lines indicate the extracellular and intracellular membrane surfaces. The black arrow indicates the signaling pathway from the orthosteric drug binding site to the intracellular surface. In A_{2A}AR, signaling has been correlated in the present work with local polymorphisms at the intracellular tips of the helices I and VI. In A_{2A}AR[D52N], signaling to the intracellular surface is quenched (Massink et al., 2014); the broken arrow indicates that an NMR-detectable structural response to variable efficacy of the bound drug was observed. The connection between the toggle switch Trp246$^{6.48}$ and the allosteric switch at Asp52$^{2.50}$ is supported by the observation of a strong interplay between these two centers in the present work.